Nonlinear Optics to Glucose Sensing: Multifunctional Nitrogen and Boron Doped Carbon Dots with Solid-State Fluorescence in Nanoporous Silica Films

Wycliffe Kiprop Kipnusu,* Carlos Doñate-Buendía, Mercedes Fernández-Alonso, Jesús Lancis, and Gladys Mínguez-Vega

Multifunctional triple color photoluminescent (PL) nitrogen–boron doped carbon quantum dots (CQDs) with high quantum yield (QY) of 58% are fabricated by one step femtosecond pulsed laser irradiation of a single precursor (2-aminopyrimidine-5-boronic acid) in solution. In situ generated non-linear and linear emissions are used to monitor CQDs formation which results in enhanced second harmonic generation, two photon absorption (2PA), and linear fluorescence; implying triple mode emission. These CQDs present blue, green, and possible red color rendering which are mostly independent to the respective excitation wavelengths (λ) with large stokes shift of 100 nm. Solid-state photoluminescence with QY of 46% is achieved by incorporating CQDs into thin transparent nanoporous silica (pSiO$_2$) films (thickness 50 μm) to form a CQDs-pSiO$_2$ composite which exhibits reverse saturable absorption at $\lambda = 800$ nm with 2PA coefficient and excited state absorption cross-section of 4.94×10^{-10} m W^{-1} and 6.23×10^{-17} cm^2, respectively. CQDs-pSiO$_2$ is also sensitive to glucose concentration down to 1.0 mg dL^{-1} in a wide linear range up to 100 mg dL^{-1}. This work therefore demonstrates facile, controllable, and up-scalable bottom-up fabrication of CQDs forming multifunctional solid-state CQDs-pSiO$_2$ with proven application in optical limiting and glucose sensing.

Photoluminescent carbon quantum dots (CQDs) are taking center stage in many applications such as biomedicine,[1] optronics, biological imaging,[2] theranostics,[3] energy storage, molecular sensing, photocatalysis,[4] and photoconversion.[5] This is because of their attractive properties including high photostability, biocompatibility, low toxicity, environmental friendliness, high water solubility, facile synthetic routes, easily

tunable photoluminescence (PL), as well as cheap and readily available precursor sources. Consequently, CQDs now occupy many frontiers of nanotechnology. Nevertheless, several challenges that hinder their full exploitation still exist, for instance, there is minimum degree of control of optical properties and morphologies during their formation. Additionally, CQDs produced from mixtures of starting precursor materials pose impurity problems to their specific applications. Furthermore, aggregation induced PL quenching of CQDs has limited their highly desired applications in the solid state. This is because in colloidal state, nature of solvent media and PH easily influence optical properties of CQDs,[6] which is unwarranted for their function as bio/chemical sensors. Herein, we present facile synthesis of multifunctional CQDs by femtosecond laser ablation of single precursor molecules in solution with feasibility of in situ monitoring and their incorporation into mesoporous silica films for solid-state applications.

Fast and easy preparation of CQDs with high purity and high fluorescence (FL) quantum yield (QY) is essential for their applications in bio/chemical sensing. In this article, emphasis is on versatile CQDs that are capable of sensing glucose molecules among other applications. Most glucose sensors are based on electrochemical technique[7] with recent studies emphasizing non-enzymatic electrochemical glucose sensing.[8–10] Detection of glucose from FL signal of CQDs is also an active area of research.[11,12] Because of its superior sensitivity, FL-based glucose sensing has great potential for ultimate design of non-invasive detection of glucose in biological fluids such as tears, sweat, and saliva where glucose concentration is about one order of magnitude lower than in blood. Non-invasive glucose sensing would be a boon to diabetic patients struggling with finger pricking method. Boronic acids are promising molecules for non-enzymatic FL detection of glucose because they form sensitive and specific reversible covalent complexes with 1,3 diols of glucose molecules.[13]

To obtain boronic acid doped CQDs, we employed femtosecond (fs) pulsed laser ablation of 2-aminopyrimidine-5-boronic acid (2-APBA) in solution in a one step process without

W. K. Kipnusu, C. Doñate-Buendía, M. Fernández-Alonso,
J. Lancis, G. Mínguez-Vega
GROC UJI
Institute of New Imaging Technologies
Universitat Jaume I
Avda. Sos Baynat sn, Castellón de la Plana 12071, Spain
E-mail: wycliffe@uji.es

⬤ID The ORCID identification number(s) for the author(s) of this article can be found under https://doi.org/10.1002/ppsc.202000093.

further additives. We used an fs laser with center wavelength (λ) 800 nm, pulse width 30 fs, repetition rate 1 KHz, pulse energy 0.15 mJ, and peak irradiance of about 10^{14} W cm^{-2} achieved with a focusing lens of focal length 75 mm. Under these conditions, filamentation occurred at the start of irradiation process owing to the fact that laser power at the focal spot is much higher than critical power (about 10^6 W) required for self-focusing in most transparent solids and liquids.[14] Filamentation appears due to dynamic counterbalance between self-focusing and defocusing of intense laser beam by optical Kerr effects and self-generated plasma, respectively. This equilibrium also clamps laser intensity inside the filament core to a constant value,[15] which is an important phenomenon because it leads to self-control of processing conditions. In this context, the laser beam causes molecular breakdown and possible reorganization into nanoparticles through photochemical process. Most laser synthesis of CQDs have been done using top-down approach involving fragmentation of larger carbonaceous materials into sizes of less than 10 nm.[16,17] However, bottom-up fabrication of CQDs mostly done through hydrothermal treatment[18–20] offer more advantages such as possibility to achieve high QYs and flexible choice of readily available cheap precursor sources.[21,22] Bottom-up laser synthesis of CQDs from transparent solutions is particularly useful because it provides additional feasible options to monitor the process in real time by capturing light emissions during laser irradiation. This is also an environmentally green method which limits waste and enables easy in situ surface functionalization of CQDs with surrounding molecular moieties.[23–25] This technique also facilitates optimization of non-linear optical (NLO) processes.

In this article, we demonstrate for the first time, the possibility to fabricate triple color emissive nitrogen/boron doped CQDs from a single precursor in solution by use of single step femtosecond pulsed laser irradiation. This approach also presents new feasible option to optimize fabrication of CQDs and NLO processes including second harmonic generation (SHG) and two photon absorption (2PA). Additionally, solid-state fluorescence of CQDs in nanoporous silica films is presented. The obtained CQDs are stable against photobleaching and are suitable for glucose sensing and optical limiting applications.

The CQDs fabrication process employed in this work is illustrated in **Figure 1**a, which depicts focused fs pulse laser beam interacting with 2-APBA molecules in solution and emitting green and blue up-converted light whose intensities change with time. Moreover, the sample was illuminated by a laser pointer (wavelength, λ = 405 nm) which resulted in green FL that also increased with fs irradiation time. We utilized electronically controlled shutters in order to separately record these emissions for in situ monitoring transformations leading to formation of CQDs. A detailed setup of this process is shown in Figure S1, Supporting Information. Additionally, we carried out Fourier transform infra-red (FTIR) spectroscopy and mass
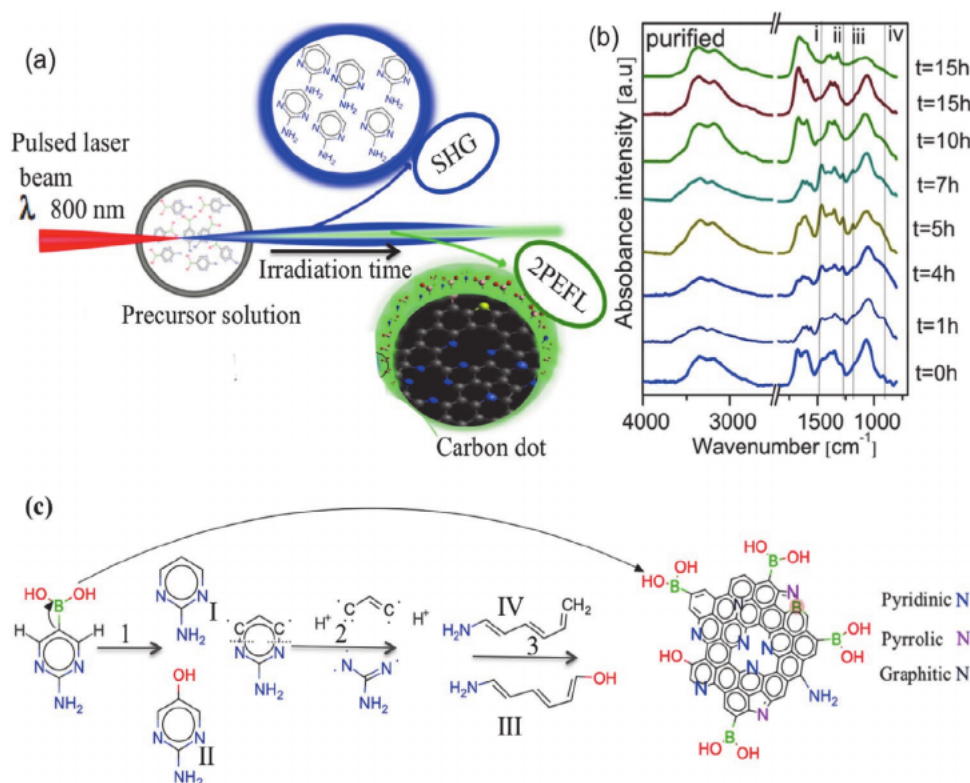

Figure 1. a) Schematic diagram of pulsed laser fabrication of carbon quantum dots (CQDs) from solution of 2-APBA showing in situ non-linear emission of two-photon excited fluorescence (2PEFL) and second harmonic generation (SHG). b) Fourier transform infrared (FTIR) spectra of the sample collected at different irradiation time as indicated. The top spectrum is from the CQDs after purification by centrifugation, filtration, and dialysis. The details of FTIR absorption peaks (i–iv) are discussed in the text. c) Scheme of production of CQDs by femtosecond pulsed laser ablation of 2-aminopyrimidine-5-boronic acid.
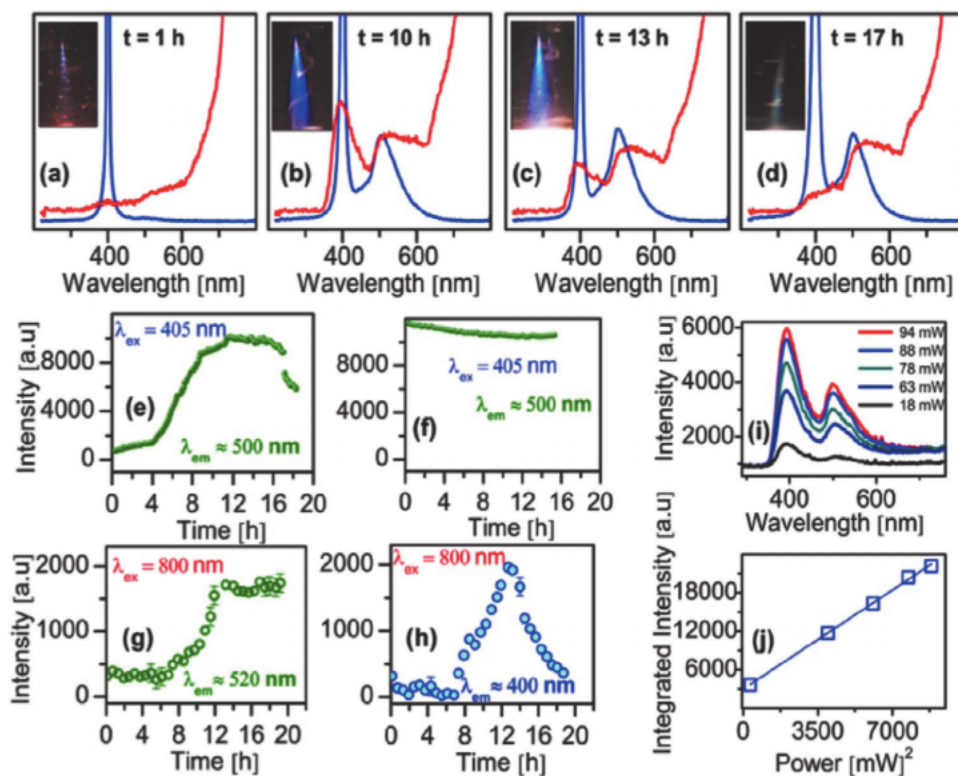
2000093 (2 of 9)

Figure 2. a–d) Spectra of in situ emissions from 2-APBA sample in solution when excited at $\lambda = 405$ nm (blue) and near infra-red, IR ($\lambda = 800$ nm) femtosecond (fs) pulsed laser (red) at the selected time during fabrication of carbon quantum dots (CQDs); insets: optical images of the emissions during excitation by the fs laser. e) Intensity of the peak emission at $\lambda = 500$ nm as a function of processing time during excitation by UV ($\lambda = 405$ nm) laser. f) Photostability of as prepared CQDs over a period of 15 h of continuous irradiation at $\lambda = 405$ nm. g) Intensity of in situ two-photon fluorescence peak at $\lambda = 520$ nm versus time when excited by fs laser ($\lambda = 800$ nm). h) Intensity of in situ emission peak at $\lambda = 400$ nm or second harmonic generation (SHG) as a function of processing time. i) Emission spectra with different laser powers by a femtosecond pulse laser (800 nm) for a sample collected after 10 h of fabrication time. j) Relationship between the intensity of the emission at $\lambda = 400$ nm or SHG and the square of laser power.

spectroscopy measurements for samples taken at different stages of fs laser fabrication. The data in Figure 1b show evolution of FTIR spectra with time. The IR absorption peak labeled (i) at 1470 cm^{-1} is attributed to C−C stretching and C−H vibrations of skeleton pyrimidine rings.[26] Other IR peaks at ii) 1257, iii) 1176, and iv) 950 cm^{-1} are ascribed to C−NH$_2$ vibrations of amino groups, C−O stretching vibrations, and B−OH wagging vibrations, respectively.[27] These IR absorption peaks (i–iii) disappear after about 10 h of fs irradiation and are therefore related to precursor material and intermediate structures. Similarly, mass spectroscopy results (Figure S2, Supporting Information) showed progressive decay of signal at m/z 140 which is due to precursor adduct and appearance of new peaks attributed to transitory compounds I and II shown in Figure 1c.

In order to gain more insight into this process, we continuously recorded the spectra (without any filters) of the in situ light emissions due to fs laser irradiation and the illumination by a laser pointer ($\lambda = 405$ nm). The evolution of the spectra (**Figure 2**a–d) of UV light of wavelength 405 nm (blue) and the fs pulsed laser beam (red) show progressive increase in linear FL emitted at around 520 nm (blue spectra), SHG at 400 nm, and two photon excited fluorescence (2PEFL) which also appears at 520 nm (red spectra). This is corroborated by optical images taken when blue laser pointer was switched off and at different times of irradiation as indicated. We analyzed inten-

sity of each of these peaks after every 10 min and plotted the results as a function of time as shown in Figure 2e,g,h. Intensity of both SHG and 2PEFL increased by about three orders of magnitude but ultimately SHG diminished while 2PEFL remained relatively constant (Figure 2h,g) implying that they are of different origins. The enhancement of SHG is attributed to intermediate compound I in Figure 1c and subsequent laser-induced alignment.[28,29] We identified compounds I and II from mass spectroscopy peaks as [m+H]$^+$ adducts at m/z 96 and 112, respectively (Figure S2, Supporting Information).

With continued fs laser ablation, compounds I and II transform to linear structures labeled III and IV through radical chain reaction (step 2). High temperature and pressure in the filament core within fs laser pulse favor pyrimidine ring opening via C−N scission to form stable open-chain radicals. This is initiated by C−H fission[30] ultimately leading to chain reaction and formation of linear conjugated radicals consisting of at least four carbon atoms.[31] The intermediate products are then carbonized (step 3) to form CQDs. Due to their volatile nature, boronic acid radical species attached immediately on the surface of CQDs.

Notably, 2-APBA fall under push–pull type of molecules. This is due to its amino group acting as electron donor (D) and boronic acid as acceptor (A) both of which are bridged by π-deficient heterocyclic conjugated pyrimidine ring. These type of molecules are capable of performing SHG[32] and 2PA.[33] Interestingly, SHG is
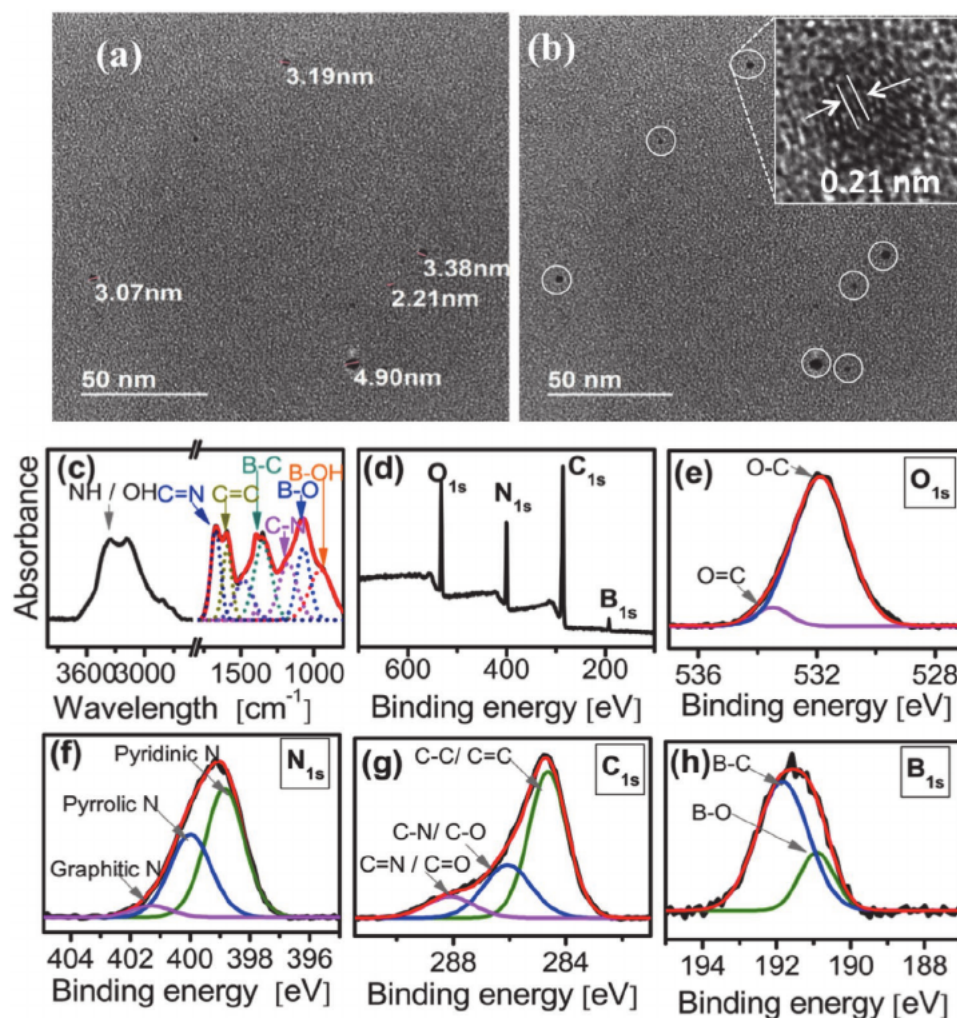
Figure 3. a) Transmission electron microscopy (TEM) image of 1000-fold diluted carbon quantum dots (CQDs); inset: b) High resolution TEM image of a representative single CQD. c) Fourier Transform Infra-red (FTIR) spectroscopy. d–h) X-ray photoelectron spectroscopy (XPS) spectra. The XPS survey spectrum of the sample indicating the presence of Oxygen (O), Nitrogen (N), Carbon (C), and Boron (B) species is shown in (d). The corresponding high-resolution XPS spectra are depicted in (e), (f), (g), and (h), respectively.

also possible from molecules having only donor moieties (push-no pull configuration)[34] as is the case with compound I discussed above. Power-dependence measurement (Figure 2I,j) confirms two-photon origin of the emissions depicted in Figure 2a–d. This implies that fs laser irradiation of similar push–pull molecules could emerge as a simple method of optimizing SHG and 2PA leading to highly functional NLO materials. Such NLO materials are in high demand for many applications including multimodal imaging,[35] optical power limiting,[36,37] nanomedicine therapy,[38] and terahertz wave generation.[39]

At the end of the fs irradiation, the color of the precursor solution changed to (pale) yellow (Figure S3, Supporting Information) indicating that CQDs are formed. These CQDs strongly emit green light when excited at $\lambda = 405$ nm and demonstrate remarkable resistance to photobleaching as illustrated in Figure 2f which show negligible loss of fluorescence intensity after about 15 h of continuous illumination at $\lambda = 405$ nm.

After purification of the prepared CQDs by filtration, centrifugation, and dialysis, we characterized them by using

transmission electron microscopy (TEM), FTIR, X-ray photoelectron spectroscopy (XPS), UV–vis absorption and fluorescence spectroscopy. TEM, FTIR, and XPS results are depicted in **Figure 3**. The average size of CQDs as measured by TEM (Figure 3a,b) is about 3 nm. High resolution TEM image in the inset of Figure 3b revealed fringes with spacing of 0.21 nm, attributed to <100> lattice distance of graphitic carbon.

The FTIR spectrum of purified CQDs (Figure 3c) show peaks at around 3345 and 3193 cm^{-1} attributed to stretching vibrations of H-bonded OH and NH moieties. IR absorption peaks appearing at 1677, 1602, and the shoulder at 1176 cm^{-1} are due to C=N, C=C, and C−N stretching vibrations, respectively. The boron containing species are detected at 1376, 1061, and 950 cm^{-1} representing IR vibrations of B−C, B−O, and B−OH groups, respectively. Consequently, the obtained CQDs contain conjugated bonds in the core structure and primary amide and boronic acid groups of precursor molecule. This is corroborated by XPS measurement.

The XPS survey spectra (Figure 3d) indicate presence of oxygen (O1s), nitrogen (N1s), carbon (C1s), and boron (B1s),
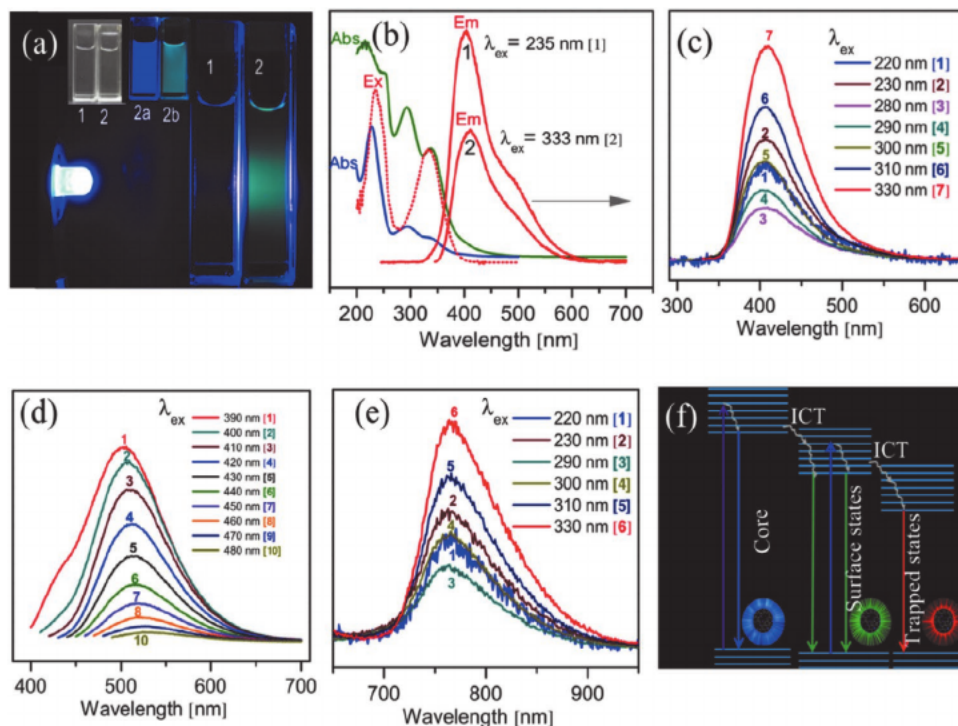
ADVANCED
SCIENCE NEWS
www.advancedsciencenews.com

Particle
& Particle Systems Characterization
www.particle-journal.com

Figure 4. a) Digital image of the precursor solution of 2-APBA (1) and after being subjected to femtosecond laser irradiation (2) when illumination of an LED of wavelength 405 nm and under ambient light (inset 1,2). Insets (2a) and (2b) are images of (2) under light of wavelength 365 and 405 nm, respectively. b) UV–vis absorption spectrum (labeled Abs) of the prepared CQDs dispersed in water. The lower absorption spectrum is from the diluted sample. FL excitation (Ex) spectrum (dotted line) shows two peaks at wavelengths 233 and 333 nm. The emission spectra at the two-excitation wavelengths are represented by curves labeled 1 and 2, respectively. c–e) FL emission spectra for different excitation wavelengths as indicated, with maxima at 407, 510, and 750 nm, respectively. To attain the same FL intensities, the detector voltage was adjusted to 430, 580, and 700 mV for the spectra in (a), (b), and (c), respectively. f) Energy diagram representation of the excitation and emission processes of CQDs indicating the role of excited state intersystem charge transfer (ICT).

species at 531, 398, 284, and 291 eV binding energies, respectively. More details about chemical bonds of these species are shown by high resolution XPS spectra (Figure 2e–h) where O1s is convoluted into two peaks at 533.5 and 531.8 eV representing O−C and O=C bonds,[40] respectively. Similarly, N1s spectrum was convoluted to three peaks at 401.3, 398.8, and 399.9 eV which are assigned to graphitic-N, pyrrolic-N, and pyridinic-N, with relative percentages of 0.05%, 38%, and 56% respectively.[40,41] Convoluted C1s spectrum (Figure 2g) show presence of C−C/C=C bonds at around 284.6 eV, C−N/C−O bonds at 286 eV, and C=N/C=O bonds at 288.6 eV.[40] In Figure 2h, B−C and B−O bonds are detected at 190.0 and 192.8 eV, respectively.[42] These XPS results further confirm that CQDs are functionalized with boronic acid species that are responsible for glucose sensing. Presence of nitrogen species are accountable for high PL quantum yields in CQDs.[43] These CQDs also exhibit interesting optical properties. When illuminated by light emitting diode (LED) of λ 405 nm, they emit green PL (2) (**Figure 4**a) that is absent in precursor solution (1). Insets (1, 2) show these two samples under ambient light.

The CQDs emit blue and green FL (in set 2a, 2b) when excited at 365 and 405 nm, respectively. This is complimented by UV–vis absorption and emission spectra (Figure 4b–e). UV–vis absorption (Abs) spectra of CQDs dispersed in water (2 mg mL^{-1}) show peaks at around 220, 250, 295, and 340 nm

and a shoulder at 400 nm (Figure 4b). After further dilution (0.002 mg mL^{-1}) the peaks at 220 and 250 nm merged into a single strong absorption peak at around 235 nm (blue spectrum). The lower wavelength peaks (220–295 nm) are attributed to π–π^* transition of conjugated C=C, and C=N bonds of CQDs core[44] and the peaks between 330–340 nm are due to n–π^* transition[45] of C−N and C−O[46] moieties. The excitation (Ex) spectrum (dotted line) exhibits two peaks which coincide with absorption peaks and results in strong emissions centered at around 435 nm and a shoulder at 500 nm when excited at λ of 235 and 333 nm respectively. This represents Stokes shift ≈100 nm, which is relatively large compared to common dyes.[47] Large Stokes shift in FL materials is a desired feature in applications such as solar concentrators,[48] super-resolution microscopy,[49] and fluorescence sensing.

Detailed FL spectra (Figure 4c–e) reveal three distinct emission windows with maxima centered at 405, 510, and 760 nm that are independent of excitation wavelengths (λ_{ex}). Using λ_{ex} between 200–330 nm results to dual (blue and red) emission at 405 and 750 nm. Single mode green emission is obtained for λ_{ex} = 400–480 nm. The red emission is ascribed to excited state charge transfer to self-trapped excitons,[50] which is accelerated by presence of N−B atoms.[51] Similarly, charge transfer from carbon core to surface states is responsible for red-shift of maxima of the blue emissions by 25 nm and

appearance of a shoulder at 500 nm (see Figure 4b; Figure S4, Supporting Information). FL in these CQDs is attributed to two mechanisms: i) direct radiative recombination after $\pi-\pi^*$ or $n-\pi^*$ transitions leading to λ_{ex} independent blue or green emission, ii) intersystem charge transfer (ICT) involving $C\pi \rightarrow N\pi^*$ and $N\pi \rightarrow B\pi^*$ followed by radiative recombination.[52] Additionally, excited electrons in the π^* orbital may be trapped by defect triplet states of pyridinic-N before they finally recombine radiatively with holes in π orbital of sp^2 boron centers. Typically, sp^2 boron is an electron-withdrawing center due to its unoccupied orbital and is therefore responsible for accelerated $N \rightarrow B$ charge transfer.[51,53] Large number of emissive trap states represented by 56% pyridinic-N centers (as deduced from XPS data) in our CQDs is responsible for near IR emission through ICT. These FL mechanisms are illustrated in Figure 4f. It shows that electrons can be excited from their ground state to higher vibrational states. During relaxation to lowest exited vibrational state where they fall back to ground state by emitting light, some electrons undergo ICT and finally emit lower energy photons which appear on longer wavelength spectrum. Typically, ICT is enhanced by the presence of donor–acceptor moieties which are often used as red emitters in LEDs and in improving organic NLO materials.[54] Due to ICT, CQDs presented here exhibit triple color emission

and are suitable for multicolor sensing, bio-imaging, as well as applications in white LED and solar cells. The blue emission has a high FL QY of 58% as determined from comparative method with quinine sulfate as reference (Figure S5, Supporting Information).

FL CQDs in the solid state is most suitable for many applications. To achieve this, we circumvented the problem of aggregation-induced FL quenching of CQDs by incorporating them in situ into transparent nanoporous silica (pSiO$_2$) films to form FL CQDs doped silica (CQDs-pSiO$_2$) composite material with FL QY of 46% measured by means of integrating sphere (Figure S6, Supporting Information). The pSiO$_2$ samples were prepared in a home-built electrochemical anodization cell, details of which can be found in ref. [55]. An optical image of blank pSiO$_2$ membrane (thickness 50 μm) delineated by a dotted line is shown in **Figure 5**a. The CQDs-pSiO$_2$ is yellow in ambient light (Figure 5b) and emits blue light under UV lamp of $\lambda = 365$ nm (Figure 5c). For ease of handling, we mounted CQDs-pSiO$_2$ samples onto a support with small openings. Optical images of these samples in ambient conditions and when illuminated by a blue laser pointer ($\lambda = 405$ nm) are shown in Figure 5d and 5e, respectively, where the CQDs-pSiO$_2$ are on the left and blank pSiO$_2$ on the right. Similar to colloidal suspension, the CQDs-pSiO$_2$ emit clear green light with
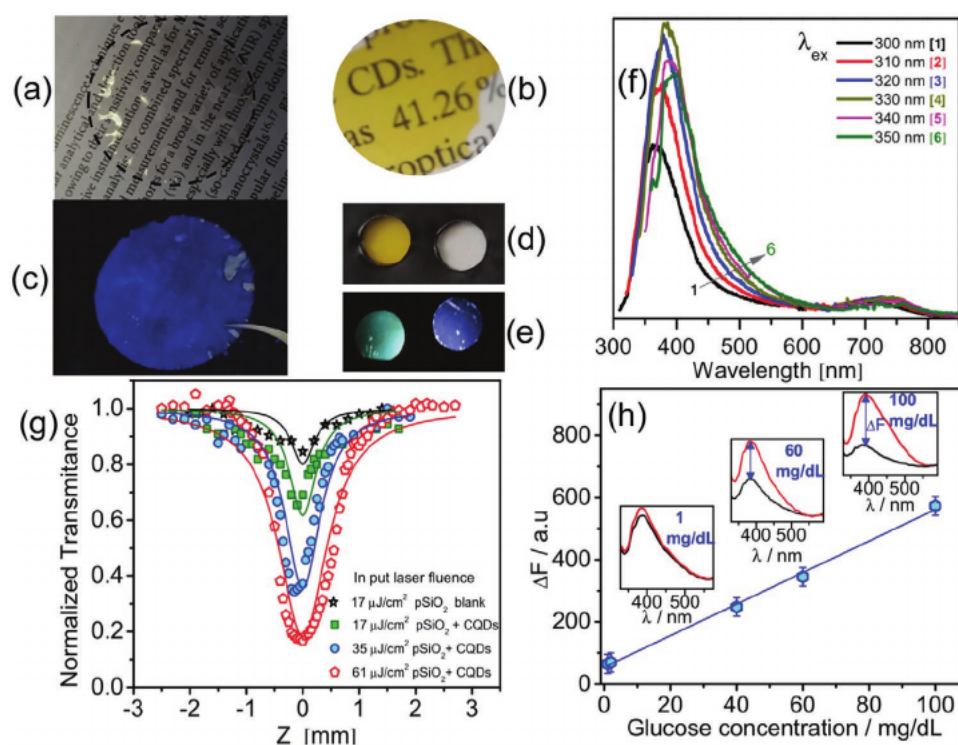

Figure 5. Optical images of: a) transparent nanoporous silica (pSiO$_2$) sheet delineated by the circular dotted line. The pSiO$_2$ has thickness of 50 μm, average pore sizes of 7 nm, and porosity of about 20%. b) pSiO$_2$ doped with carbon dots (CQDs-pSiO$_2$). c) CQDs-pSiO$_2$ under ultra-violet (UV) lamp of wavelength 365 nm. d) CQDs-pSiO$_2$ (left) and blank pSiO$_2$ (right) mounted on a support with open circular holes. The images were taken in ambient light. e) CQDs-pSiO$_2$ (left) and blank pSiO$_2$ (right) illuminated by an LED of wavelength 405 nm. f) Fluorescence spectra of CQDs-pSiO$_2$ at selected excitation wavelengths. g) Reverse saturable absorption of CQDs-pSiO$_2$ at $\lambda = 800$ nm described by normalized power transmittance versus z-position of the sample. The lines represent fits to the data as estimated by numerical expression explained in Supporting Information. h) A plot of change of fluorescence of the prepared CQDs against glucose concentration in the range 1–100 mg dL^{-1}. The inset depicts the fluorescence spectra of the CQDs before and after adding different concentrations of glucose as indicated. The fluorescence of CQDs is quenched depending on the concentration of the added glucose.

λ_{ex} = 405 nm. The representative fluorescence spectra of CQDs-pSiO$_2$ measured in an integrating sphere for λ_{ex} 300–350 nm (Figure 5f) also depict weak near infrared (750 nm) emission besides strong deep blue (400 nm) emission with QY of 46%.

Compared to solid state FL of CQDs in powder or when embedded in polymeric substrates, the method presented in this article of formulating them into thin transparent nanoporous silica films is the most convenient approach for many applications, especially in molecular sensing owing to chemical inertness of silica. Subsequently, we tested CQDs-pSiO$_2$ samples for their use in optical limiting and glucose sensing.

Optical limiting (OL) occurs when power of a pulsed laser beam decreases upon interacting with a material that has nonlinear optical properties such as multiphoton absorption, nonlinear scattering, and reflection.[56] OL materials are required for protecting human eyes and optical sensors from laser induced damages. The OL property of the obtained CQDs-pSiO$_2$ was investigated using open aperture (OA) Z-scan technique with fs pulsed laser of mean λ = 800 nm. In this method, the sample is moved across a focused laser spot as transmitted power is recorded at each step (details in Section S1, Supporting Information). In Figure 5g, normalized transmitted power is plotted as a function of position Z of the sample from focal spot for different input fluence. These results indicate that CQDs-pSiO$_2$ has strong OL property characterized by reverse saturable absorption that increases with increasing laser fluence. We attribute this phenomenon to 2PA and photogenerated excited state absorption (ESA).[57,58] From the OA Z-scan data, we obtained 2PA coefficient $\beta = 4.94 \times 10^{-10}$ m W^{-1}. Since charge diffusion and decay within fs pulse duration is negligible, β can be linked to ESA cross-section (σESA) by $\sigma\text{ESA} = \beta I_0 2\hbar\omega / F$ where I_0 and F are peak irradiance and fluence, respectively, while $\hbar\omega$ is connected to excitation photon energy.[59] From this relationship, the estimated value of σESA (6.23×10^{-17} cm^2) is within the range of σESA of materials with strong excited state transition.[57]

On the other hand, boronic acid doped CQDs are very suitable for FL detection of glucose molecules through Föster resonance energy transfer mechanism.[13,42] We employed CQDs-pSiO2 mounted on a support as shown on the left of Figure 5d to carry out fluorescence measurements of these samples in the solid state before and after adding 10 µL of glucose solutions in deionized water. The determined fluorescence change (ΔFL) shows linear dependence with glucose concentrations in a wide range (Figure 5h). Notably, our CQDs-pSiO$_2$ can sense glucose levels down to 1 mg dL^{-1}, which is in the range of glucose concentration in external assay of body fluids such as sweat,[60] and tears.[61] It therefore offers a viable opportunity for non-invasive plasma glucose monitoring that has been in the offing for long but still remains a desire for many diabetes patients suffering with finger pricking method. Test of glucose sensing of CQDs-pSiO$_2$ samples in the presence of other interfering analytes is ongoing.

In summary, we have presented a facile fabrication of nitrogen/boron doped CQDs from a single precursor molecule in solution by femtosecond laser ablation. This allowed us to monitor both non-linear (second harmonic generation, two photon absorption) and linear fluorescence (FL) in the course of CQDs formation whose mechanism is also highlighted.

The produced CQDs emit FL in blue, green, and red spectral regions at suitable excitation wavelengths. Furthermore, we have produced solid-state fluorescent composite CQDs doped silica films with demonstrated optical limiting and glucose detection down to 1.0 mg dL^{-1} over a wide linear range of 100 mg dL^{-1}. Potentially, these CQDs can find applications in many other fields such as high-resolution imaging, solar cells, and light emitting diodes.

Experimental Section

Materials: 2-APBA sample with purity of 95% was purchased from Sigma-Aldrich. Ultrapure water (resistivity 18 M Ωcm at 25 °C, Milli-Q system) was used as solvent. Two different concentrations, 0.002 and 0.05 M of 2-APBA were prepared by dissolving appropriate amounts of 2-APBA in pure water. The mixture was ultrasonicated at 60 °C using ultrasonic probe UP400s (Hielscher Ultrasonics Gmbh, Germany) for 4 h. Details for fs laser synthesis of CQDs from 2-APBA is presented in the Supporting Information.

Purification of Prepared CQDs: The fabricated CQDs were first purified by filtration using polycarbonate membrane filters (from Filter-Lab) having pore size of 0.1 µm. The sample was then centrifuged at 4000 rpm for 1 h. In order to remove small organic molecules, the sample was finally dialyzed for 24 h using 1 kDa molecular weight cut-off (MWCO) Pur-A-Lyzer mega tubes (from Sigma-Aldrich).

Fourier Transform Infrared: FTIR measurements were carried out at room temperature (about 22 °C) using a Bio-Rad FTS 6000 spectrometer from 700 to 5000 cm^{-1} with a resolution of 2 cm^{-1}. The samples were prepared on calcium fluoride (CaF$_2$) windows. First, about 10 mg of barium fluoride (BaF$_2$) powder was placed on a clean CaF$_2$ surface and mixed with about 200 µL of colloidal suspension of CQDs in water. The sample was then heated on a hot plate at 60 °C for five minutes to remove excess water. To completely remove the water content, the sample was further annealed at 100 °C in high vacuum (10^{-6} mbar) for 24 h.

X-Ray Photoelectron Spectroscopy: The surface sensitive XPS (K-ALPHA, Thermo Scientific) technique was used to probe surface states of CQDs. All spectra were collected using Al-K- radiation (1486.6 eV), monochromatized by a twin crystal monochromator, yielding a focused X-ray spot (elliptical in shape) with a major axis length of 400 µm at 3 mA × 12 kV. The alpha hemispherical analyzer was operated in the constant energy mode with survey scan pass energies of 200 eV to measure the whole energy band and 50 eV in a narrow scan to selectively measure the particular elements. XPS data were analyzed with Avantage software. A smart background function was used to approximate the experimental backgrounds while surface elemental compositions were calculated from background-subtracted peak areas. Charge compensation was achieved with the system flood gun that provides low energy electrons and low energy argon ions from a single source. The colloidal suspension of CQDs was drop cast and dried onto TEM grids for five times to ensure complete surface coverage.

Transmission Electron Microscopy: Thermionic TEM equipped with JEOL JEM 1010 emitter with 0.4 nm resolutions was used to probe the sizes and intrinsic lattice spacing of the obtained particles. Prior to the TEM measurement, the sample was dispersed onto carbon-coated copper-based TEM grid.

Optical Measurements: Fluorescence measurements were carried out using Cary (Varian) Eclipse Fluorescence spectrometer while UV–vis absorption was recorded using Cary (Varian) 500 Scan UV–vis Spectrometer UV-VIS-NIR spectrophotometer unit. 10 mm pathlength quartz cuvette was used.

Formulation of CQDs into Nanoporous Silica Films: Details of preparation of nanoporous silica (pSiO$_2$) membranes can be found in ref. [55]. In brief, pSiO$_2$ were fabricated by electrochemical etching of highly doped p-type silicon wafers in a home-built anodization cell

followed by oxidation step. The electrolyte contained hydrofluoric acid (HF-48%) and ethanol (C_2H_5OH-99%) purchased from Sigma-Aldrich and mixed in the ratio of 1:1. Current densities (j) in the range of 20–120 mA cm^{-2} were applied to obtain pore diameters between 4 and 10 nm. In situ infiltration of CQDs into $pSiO_2$ was done by placing $pSiO_2$ sheet that was supported by a glass slide placed above the surface of the precursor liquid such that the laser focus spot was in the liquid just below the lower surface of the porous silica sheet. In this way, coulomb explosion from pulsed laser causes infiltration of CQDs directly into the porous silica sheets to form a composite material referred here as CQDs doped porous silica (CQDs-$pSiO_2$). The whole sample setup was placed on a translational table as shown in Figure S1, Supporting Information.

Glucose Sensing: The prepared CDs in the solid state (CDs-$pSiO_2$) were used for glucose sensing. First the fluorescence of CDs-$pSiO_2$ (at excitation wavelength of 320 nm) was recorded using the Cary Eclipse spectrometer in order to obtain the baseline. Thereafter, 10 µL of specific glucose concentrations in water was dropped onto the CDs-$pSiO_2$ without dismounting it from the spectrometer sample holder. Fluorescence quenching was then monitored until there was no further change. The final fluorescence intensity was subtracted from the baseline. This was done for different concentration of glucose to obtain the calibration line shown in Figure 5h. Further studies on sensitivity of CDs-$pSiO_2$ to glucose in the presence of other interfering analytes and also using real tear sample assays are undergoing.

Supporting Information

Supporting Information is available from the Wiley Online Library or from the author.

Acknowledgements

Conflict of Interest

The authors declare no conflict of interest.

Keywords

[1] F. Huo, P. G. Karmaker, Y. Liu, B. Zhao, X. Yang, *Part. Part. Syst. Charact.* **2020**, *37*, 1900489.

[2] K. Hola, Y. Zhang, Y. Wang, E. P. Giannelis, R. Zboril, A. L. Rogach, *Nano Today* **2014**, *9*, 590.

[3] X. Bao, Y. Yuan, J. Chen, B. Zhang, D. Li, D. Zhou, P. Jing, G. Xu, Y. Wang, K. Holá, D. Shen, C. Wu, L. Song, C. Liu, R. Zbořil, S. Qu, *Light: Sci. Appl.* **2018**, *7*, 91.

[4] Z. Zhang, T. Zheng, X. Li, J. Xu, H. Zeng, *Part. Part. Syst. Charact.* **2016**, *33*, 457.

[5] C. Hu, M. Li, J. Qiu, Y.-P. Sun, *Chem. Soc. Rev.* **2019**, *48*, 2315.

[6] D. Pan, J. Zhang, Z. Li, C. Wu, X. Yan, M. Wu, *Chem. Commun.* **2010**, *46*, 3681.

[7] C. Chen, Q. Xie, D. Yang, H. Xiao, Y. Fu, Y. Tan, S. Yao, *RSC Adv.* **2013**, *3*, 4473.

[8] F. Xie, X. Cao, F. Qu, A. M. Asiri, X. Sun, *Sens. Actuators, B* **2018**, *255*, 1254.

[9] Y. Liu, X. Cao, R. Kong, G. Du, A. M. Asiri, Q. Lu, X. Sun, *J. Mater. Chem. B* **2017**, *5*, 1901.

[10] D. Zhou, X. Cao, Z. Wang, S. Hao, X. Hou, F. Qu, G. Du, A. M. Asiri, C. Zheng, X. Sun, *Chem. - Eur. J.* **2017**, *23*, 5214.

[11] D. C. Klonoff, *J. Diabetes Sci. Technol.* **2012**, *6*, 1242.

[12] M.-S. Steiner, A. Duerkop, O. S. Wolfbeis, *Chem. Soc. Rev.* **2011**, *40*, 4805.

[13] G. Fang, H. Wang, Z. Bian, J. Sun, A. Liu, H. Fang, B. Liu, Q. Yao, Z. Wu, *RSC Adv.* **2018**, *8*, 29400.

[14] A. Brodeur, S. L. Chin, *Phys. Rev. Lett.* **1998**, *80*, 4406.

[15] W. Liu, S. Petit, A. Becker, N. Aközbek, C. M. Bowden, S. L. Chin, *Opt. Commun.* **2002**, *202*, 189.

[16] R. Wang, K.-Q. Lu, Z.-R. Tang, Y.-J. Xu, *J. Mater. Chem. A* **2017**, *5*, 3717.

[17] C. Doñate-Buendia, R. Torres-Mendieta, A. Pyatenko, E. Falomir, M. Fernández-Alonso, G. Mínguez-Vega, *ACS Omega* **2018**, *3*, 2735.

[18] Y. Guo, Y. Chen, F. Cao, L. Wang, Z. Wang, Y. Leng, *RSC Adv.* **2017**, *7*, 48386.

[19] S. Liu, J. Tian, L. Wang, Y. Zhang, X. Qin, Y. Luo, A. M. Asiri, A. O. Al-Youbi, X. Sun, *Adv. Mater.* **2012**, *24*, 2037.

[20] W. Lu, X. Qin, S. Liu, G. Chang, Y. Zhang, Y. Luo, A. M. Asiri, A. O. Al-Youbi, X. Sun, *Anal. Chem.* **2012**, *84*, 5351.

[21] S. N. Baker, G. A. Baker, *Angew. Chem., Int. Ed.* **2010**, *49*, 6726.

[22] Y. Wang, A. Hu, *J. Mater. Chem. C* **2014**, *2*, 6921.

[23] D. Zhang, B. Gökce, S. Barcikowski, *Chem. Rev.* **2017**, *117*, 3990.

[24] J. Xiao, P. Liu, C. X. Wang, G. W. Yang, *Prog. Mater. Sci.* **2017**, *87*, 140.

[25] C. Doñate-Buendía, M. Fernández-Alonso, J. Lancis, G. Mínguez-Vega, *Photonics Res.* **2019**, *7*, 1249.

[26] W. O. George, P. S. McIntyre, D. J. Mowthorpe, *Infrared Spectroscopy*, John Wiley & Sons Inc., Chichester, NY **1987**.

[27] M. K. Smith, B. H. Northrop, *Chem. Mater.* **2014**, *26*, 3781.

[28] S. Fleischer, Y. Khodorkovsky, E. Gershnabel, Y. Prior, I. S. Averbukh, *Isr. J. Chem.* **2012**, *52*, 414.

[29] A. S. Chatterley, C. Schouder, L. Christiansen, B. Shepperson, M. H. Rasmussen, H. Stapelfeldt, *Nat. Commun.* **2019**, *10*, 133.

[30] S. W. Wren, K. M. Vogelhuber, J. M. Garver, S. Kato, L. Sheps, V. M. Bierbaum, W. C. Lineberger, *J. Am. Chem. Soc.* **2012**, *134*, 6584.

[31] J. H. Kiefer, Q. Zhang, R. D. Kern, J. Yao, B. Jursic, *J. Phys. Chem. A* **1997**, *101*, 7061.

[32] J. E. Reeve, H. L. Anderson, K. Clays, *Phys. Chem. Chem. Phys.* **2010**, *12*, 13484.

[33] S. Achelle, S. Kahlal, A. Barsella, J.-Y. Saillard, X. Che, J. Vallet, F. Bureš, B. Caro, F. R. Guen, *Dyes Pigm.* **2015**, *113*, 562.

[34] I. López-Duarte, J. E. Reeve, J. Pérez-Moreno, I. Boczarow, G. Depotter, J. Fleischhauer, K. Clays, H. L. Anderson, *Chem. Sci.* **2013**, *4*, 2024.

[35] R. Misri, in *Molecular Imaging Techniques: New Frontiers*, Future Science Ltd, London, UK **2013**, pp. 162–176.

[36] P. Chantharasupawong, R. Philip, N. T. Narayanan, P. M. Sudeep, A. Mathkar, P. M. Ajayan, J. Thomas, *J. Phys. Chem. C* **2012**, *116*, 25955.

[37] X. Tian, R. Wei, Q. Guo, Y.-J. Zhao, J. Qiu, *Adv. Mater.* **2018**, *30*, 1801638.

[38] W. Fan, W. Bu, J. Shi, *Adv. Mater.* **2016**, *28*, 3987.

[39] J. Zhao, W. Chu, Z. Wang, Y. Peng, C. Gong, L. Lin, Y. Zhu, W. Liu, Y. Cheng, S. Zhuang, Z. Xu, *ACS Photonics* **2016**, *3*, 2338.

ADVANCED
SCIENCE NEWS
www.advancedsciencenews.com

Particle
& Particle Systems Characterization
www.particle-journal.com

[40] H. Ding, S.-B. Yu, J.-S. Wei, H.-M. Xiong, *ACS Nano* **2016**, *10*, 484.

[41] X. Miao, D. Qu, D. Yang, B. Nie, Y. Zhao, H. Fan, Z. Sun, *Adv. Mater.* **2018**, *30*, 1704740.

[42] P. Shen, Y. Xia, *Anal. Chem.* **2014**, *86*, 5323.

[43] J. Hou, W. Wang, T. Zhou, B. Wang, H. Li, L. Ding, *Nanoscale* **2016**, *8*, 11185.

[44] S. Bhattacharyya, F. Ehrat, P. Urban, R. Teves, R. Wyrwich, M. Döblinger, J. Feldmann, A. S. Urban, J. K. Stolarczyk, *Nat. Commun.* **2017**, *8*, 1401.

[45] J. Shao, S. Zhu, H. Liu, Y. Song, S. Tao, B. Yang, *Adv. Sci.* **2017**, *4*, 1700395.

[46] K. Holá, M. Sudolská, S. Kalytchuk, D. Nachtigallová, A. L. Rogach, M. Otyepka, R. Zbořil, *ACS Nano* **2017**, *11*, 12402.

[47] T.-B. Ren, W. Xu, W. Zhang, X.-X. Zhang, Z.-Y. Wang, Z. Xiang, L. Yuan, X.-B. Zhang, *J. Am. Chem. Soc.* **2018**, *140*, 7716.

[48] C. Yang, J. Zhang, W.-T. Peng, W. Sheng, D. Liu, P. S. Kuttipillai, M. Young, M. R. Donahue, B. G. Levine, B. Borhan, R. R. Lunt, *Sci. Rep.* **2018**, *8*, 1.

[49] H. Blom, J. Widengren, *Chem. Rev.* **2017**, *117*, 7377.

[50] M. Fu, F. Ehrat, Y. Wang, K. Z. Milowska, C. Reckmeier, A. L. Rogach, J. K. Stolarczyk, A. S. Urban, J. Feldmann, *Nano Lett.* **2015**, *15*, 6030.

[51] M. K. Barman, B. Jana, S. Bhattacharyya, A. Patra, *J. Phys. Chem. C* **2014**, *118*, 20034.

[52] L. Tang, R. Ji, X. Li, K. S. Teng, S. P. Lau, *J. Mater. Chem. C* **2013**, *1*, 4908.

[53] Y. Li, H. Meng, T. Liu, Y. Xiao, Z. Tang, B. Pang, Y. Li, Y. Xiang, G. Zhang, X. Lu, G. Yu, H. Yan, C. Zhan, J. Huang, J. Yao, *Adv. Mater.* **2019**, *31*, 1904585.

[54] Y. Li, T. Liu, H. Liu, M.-Z. Tian, Y. Li, *Acc. Chem. Res.* **2014**, *47*, 1186.

[55] W. K. Kipnusu, M. Elsayed, R. Krause-Rehberg, F. Kremer, *J. Chem. Phys.* **2017**, *146*, 203302.

[56] D. Dini, M. J. F. Calvete, M. Hanack, *Chem. Rev.* **2016**, *116*, 13043.

[57] Q. Bellier, N. S. Makarov, P.-A. Bouit, S. Rigaut, K. Kamada, P. Feneyrou, G. Berginc, O. Maury, J. W. Perry, C. Andraud, *Phys. Chem. Chem. Phys.* **2012**, *14*, 15299.

[58] J.-J. Wu, Y.-R. Tao, J.-N. Wang, Z.-Y. Wu, L. Fan, X.-C. Wu, *Nanoscale* **2016**, *8*, 10371.

[59] E. W. van Stryland, M. Sheik-Bahae, A. A. Said, D. J. Hagan, *Prog. Cryst. Growth Charact. Mater.* **1993**, *27*, 279.

[60] Y. J. Hong, H. Lee, J. Kim, M. Lee, H. J. Choi, T. Hyeon, D.-H. Kim, *Adv. Funct. Mater.* **2018**, *28*, 1805754.

[61] J. T. La Belle, A. Adams, C.-E. Lin, E. Engelschall, B. Pratt, C. B. Cook, *Chem. Commun.* **2016**, *52*, 9197.

2000093 (9 of 9)